arXiv:1609.08358v1 [cond-mat.str-el] 27 Sep 2016

Spin-wave dynamics in FeGe helimagnet: studied by small-angle neutron scattering

S.-A. Siegfried,[1] A. S. Sukhanov,[2,3] E. V. Altynbaev,[2,3] D. Honnecker,[4]
A. Heinemann,[1] A. V. Tsvyashchenko,[5] and S. V. Grigoriev[2,3]

[1] *German Engineering Materials Science Centre (GEMS) at Heinz Maier-Leibnitz Zentrum (MLZ), Helmholtz-Zentrum Geesthacht GmbH, Lichtenbergstr. 1, 85747 Garching bei München, Germany*
[2] *Petersburg Nuclear Physics Institute, Gatchina, St-Petersburg, 188300, Russia*
[3] *Saint-Petersburg State University, Ulyanovskaya 1, Saint-Petersburg, 198504, Russia*
[4] *Institute Laue Langevin, Grenoble, 38042 Grenoble, Cedex 9, France*
[5] *Institute for High Pressure Physics, Russian Academy of Sciences, 142190 Troitsk, Moscow, Russia*

(Dated: September 28, 2016)

We have studied the spin-wave stiffness of the Dzyaloshinskii-Moriya helimagnet FeGe in a temperature range from 225 K up to $T_C \approx 278.7$ K by small-angle neutron scattering. The method we have used is based on [S. V. Grigoriev et al. Phys. Rev. B **92** 220415(R) (2015)] and was extended here for the application in polycrystalline samples. We confirm the validity of the anisotropic spin-wave dispersion for FeGe caused by the Dzyaloshinskii-Moriya interaction. We have shown that the spin-wave stiffness A for FeGe helimagnet decreases with a temperature as $A(T) = 194(1-0.7(T/T_C)^{4.2})$ meVÅ^2. The finite value of the spin-wave stiffness $A = 58$ meVÅ^2 at T_C classifies the order-disorder phase transition in FeGe as being the first order one.

PACS numbers: 61.12.Ex, 75.30.Ds, 75.25.-j

I. INTRODUCTION

The cubic B20 compounds have a noncentrosymmetric crystal structure described by the $P2_13$ space group. The lack of a symmetry center of the crystal structure produces the chiral spin-spin Dzyaloshinskii-Moriya (DM) interaction[1,2]. According to the model by Bak and Jensen[3] and Kataoka[4], the major ferromagnetic exchange interaction J, together with the DM interaction D produces a (homochiral) structure in these systems below T_c. The energy landscape in these systems is given by J and D, which are balanced via the helix wave vector $k_s = D/J$. The anisotropic exchange interaction has been added to the model, changing slightly the value and fixing the direction of the wave vector $\boldsymbol{k}_s$ along the principle cubic axis. As noticed by Kataoka and co-workers[4] and Maleyev and co-workers[5], the cubic anisotropy can play an important role in the case of relative small values of the helix wave vector k_s. If the anisotropic energy getting comparable to the DM interaction, it can destabilize the entire helix structure and stabilizes instead the ferromagnetic state.

The external magnetic field H_{c1} is needed to rotate the helix wave vector $\boldsymbol{k}_s$ towards the field direction and, therefore, it is a measure for the anisotropy of the system. According to[6], the energy difference between the conical and the collinear full-polarized (FP) state can be directly measured by the second critical field H_{c2}. This energy is equal to $g\mu_B H_{c2} \approx Ak_s^2$, where $A = J \cdot S \cdot a^2$ is the spin-wave stiffness, S is the ordered spin, and a is the lattice constant. The experimental parameters k_s, H_{c1}, H_{c2} and S describe completely the magnetic system of such compounds.

The compound FeGe shows a significant difference in the parameters of the magnetic structure compared to the other B20 helimagnet MnSi[7,8]. The helix length is nearly four times higher and equal to $\lambda_h \approx 700$ Å, and the ordering temperature $T_C \approx 278.7$ K is nearly ten times higher than the T_C for MnSi. As to the anisotropic interactions the helix wave vector is pinned along the [111] direction in MnSi at all temperatures below $T_C \approx 29.5$ K, whereas the helix wave vector in FeGe is pinned along the [100] direction in the high-temperature range between $T_C = 278.7$ K and $T_{2\downarrow}$=211 K/$T_{2\uparrow}$=245 K and rotates towards the [111] direction in the low-temperature part of the ordered phase for $T < T_{2\downarrow,\uparrow}$. According to the Bak and Jensen model a temperature driven rotation of the spiral from the [100] to the [111] goes along with a change of the sign of the second order gradient in the free energy expansion. Nevertheless, magnetization measurements indicated that the rotation of the helix axis at $T_{2\downarrow,\uparrow}$ can be explained by an interplay of constants of 4th and 6th terms of the cubic anisotropy[9].

While the spin-wave dynamic of MnSi has been intensively studied in the past[10–16], it was never the case for FeGe, due to the lack of a sufficient large amount of single crystalline samples, which is necessary for the triple axis spectroscopy (TAS). The recently proposed method[16] to determine the spin-wave stiffness in the helical magnets based on DM interaction in the FP state, using polarized small-angle neutron scattering (SANS), can be extended to be used for the polycrystalline FeGe compounds. This method was originally developed and applied to measure the spin-wave stiffness in ferromagnetic compounds[17–21]. The presence of the DM chiral interaction leads to the chirality of the spin-waves in FP state of helimagnets. This fact is related to the completely anisotropic dispersion relation of magnons, which reads

$$\epsilon_{\boldsymbol{q}} = A\left(\boldsymbol{q} - \boldsymbol{k}_s\right)^2 + H - H_{c2} \qquad (1)$$

for the magnetic field above the critical value H_{c2}[22]. It can be analytically shown that the inelastic scattering of the neutrons in this case is concentrated mostly around the momentum transfers corresponding to $\pm\boldsymbol{k}_s$ within two narrow cones limited by the cut-off angle θ_C for the energy gain/energy loss, respectively[16]. The cut-off angle is connected to the spin-wave stiffness via the dimensionless parameter $\theta_0 = (2Am_n)^{-1}$:

$$\theta_C^2(H) = \theta_0^2 - \frac{\theta_0}{E_i}H + \theta_B^2, \qquad (2)$$

where m_n is the neutron mass, θ_B is the Bragg angle of the scattering on the spin spiral with the length $2\pi/k_s$, and E_i denotes the energy of the incident neutrons.

Here we assume conditions $\omega \ll E_i$ and $\omega \ll T$ to be fulfilled in the limit of small-angle neutron scattering. The first condition allows one to split momentum transfer into elastic component perpendicular to $\boldsymbol{k}_i$ and inelastic one parallel to $\boldsymbol{k}_i$. Bose factor $[1-\exp(-\omega/T)]^{-1}$ can be replaced by T/ω accounting for the second condition. Despite of being ω-odd, the cross section of the inelastic scattering being integrated over the energy transfer contains the polarization-dependent part due to the peculiarity of the aforementioned asymmetric dispersion relation. As was demonstrated in[16], one can distinguish the scattering from the helimagnons in a homochiral crystalline sample using polarized neutrons in SANS experiment.

In this paper we show the possibility to measure the SW stiffness in the polycrystalline samples using non-polarized neutrons. As the sample contains both left and right crystallites, it is, therefore, not possible to demonstrate the chiral nature of the spin-wave scattering. Nevertheless, it is possible to detect two circles on a scattering map with radius θ_C and centered at the Bragg peak θ_B. The spin-wave stiffness A is measured in the temperature range below T_C by finding the cut-off angle in accordance to Eq.2.

This paper is organized in the following way: Sections II and III give the results of the small-angle neutron scattering measurements of the FeGe compound. Section IV presents the conclusions.

II. ELASTIC SMALL-ANGLE NEUTRON MEASUREMENTS

The SANS experiment was performed at the D11 instrument at the ILL (Grenoble, France). An unpolarized beam with a mean wavelength of $\lambda = 0.6$ nm was used. A magnetic field (0.0 - 0.5 T) was applied perpendicular to the incident beam. The FeGe sample with the mass of 0.1 g was the same as used in our previous work[23]. It was synthesized using the high pressure method (see[24] for details).

Typical SANS map for $T = 250$ K and $H \gtrsim H_{c1} = 0.075$ T is shown in Fig.1 (a). Several Bragg peaks appear on the left and right sides of the scattering map, where the center of the map corresponds to $Q_x = 0, Q_y = 0$. The two peaks closest to the center are from the helical structure at $Q = \pm 0.09$ nm^{-1}. The others are clearly the higher orders of multiple scattering. The spiral wave vector is aligned to the direction of the magnetic field.

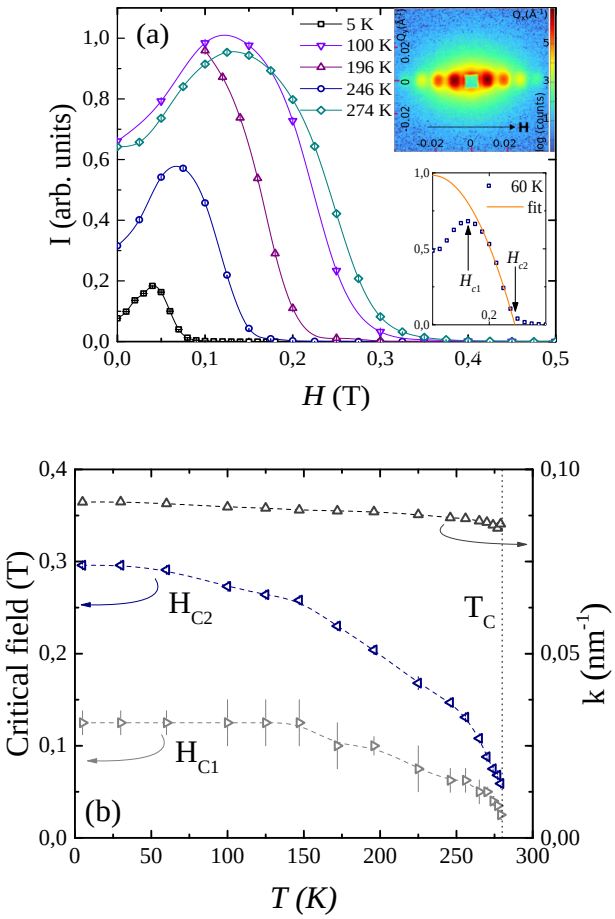

FIG. 1: (color online). (a) Typical SANS scattering pattern from a monodomain helix structure below H_{c2}, $T = 250$ K and a magnetic field $H = 0.075$ T. Integral intensity of the Bragg peak against the magnetic field at different temperatures between 5 and 274 K. Solid lines are guide for eyes. The upper insert shows a typical SANS scattering pattern from a monodomain helix structure below H_{c2}, $T = 250$ K and a magnetic field $H = 0.075$ T. The bottom insert shows an illustration of the determination of the H_{c2} at 60 K. The BJ model is used to provide the fitting function (see the text for more details). (b) The temperature dependence of the value of the helix wavevector k_s and both critical field $H_{c1,2}$. Dashed lines are guide for eyes.

Fig.1 (b) represents the integrated intensities of the Bragg peak I at $Q = \pm 0.09$ nm^{-1} as function of the field for different temperatures between 5 K and $T_C \approx 278.7$ K. The sample has been cooled down from T_C. The cooling has been stopped at 16 different temperatures in-between and a field scan with increasing magnetic field was performed at each temperature. As it is

shown in the insert, the first critical field H_{c1} is defined as a point of the maximal intensity, this is the point where all spirals are aligned along the field. The difference to the previously used method[23] for $Fe_{1-x}Co_xGe$ is worth mentioning, where we determined H_{c1} as the starting point for the increasing intensity, corresponding to the spirals starts aligning along the field direction. The second critical field H_{c2} is determined from the zero point of the fitting function according to the Bak-Jensen model. The model predicts that the cone angle α, counted from the helix plane, increases with the field as[6]:

$$\sin\alpha = \frac{H}{H_{c2}}. \tag{3}$$

Thus, the intensity of elastic scattering subsides $I \sim \cos^2\alpha \sim 1-(H/H_{c2})^2$. However, a tail of the intensity can be still observed above H_{c2} (Fig. 1 (a)). This tail is better pronounced at the low temperatures, while it becomes invisible in the high-temperature region. The phenomenon may be caused by influence of the cubic anisotropy that makes the critical field H_{c2} depending on orientation of the applied field with respect to the principal crystallographic axes[5]. The magnetic structure in the randomly oriented crystallites undergo the phase transition to the field polarized state at different strength of the field from the minimal $H_{c2} = Ak_s^2 - 8G/(3S)$ to maximal value $H_{c2} = Ak_s^2 + 4G/S$, where G is the constant of the cubic anisotropy.

The helix wave vector $|\boldsymbol{k}_s|$ has been determined as a center of the Gaussian function fitting the helical Bragg peak in zero magnetic field for each temperature. The temperature dependence of the helix wave vector is shown in Fig.1 (b), it is nearly constant and equal to 0.09 nm^{-1} in the whole temperature range. Furthermore, the $H-T$ phase diagram for FeGe between 5 K and T_C is shown in Fig.1 (b). The second critical field H_{c2} decreases slowly from a maximum value of 0.3 T at low temperature and tends to zero at T_C. The first critical field H_{c1} stays roughly constant at 0.1 T between 5 K and 180 K and decreases with further temperature increase towards zero at T_C. As it was mentioned, the H_{c2} is the measure of the difference in energies of the spiral state and the FP state and is equal to Ak_s^2. As far as k_s shows no change, temperature decrease of H_{c2} is expected to be driven by decrease of A and is related to the softening of the magnetic structure with the temperature. Meanwhile the mechanism standing behind the temperature changing of the H_{c1} remains less clear.

III. SMALL-ANGLE NEUTRON MEASUREMENTS OF THE SPIN-WAVE STIFFNESS

The insert of Figure 2 shows a typical SANS map for FeGe, which is taken above H_{c2}. As the field reaches H_{c2} the elastic scattering disappears and only the inelastic scattering centered at $\boldsymbol{Q} = \pm\boldsymbol{k}_s$ remains. This scattering

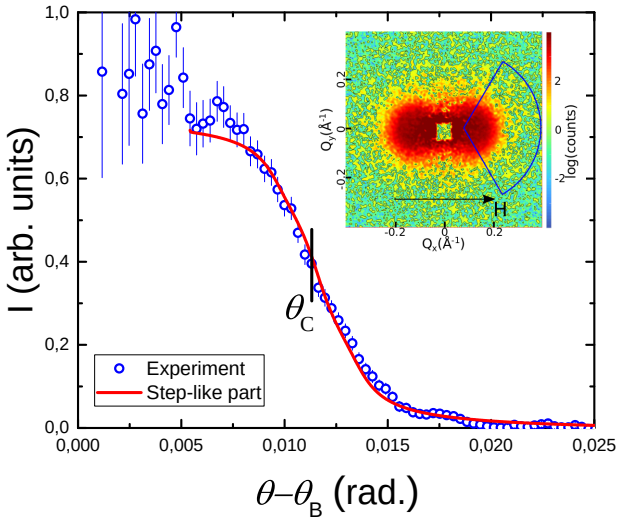

FIG. 2: (color online).The averaged intensity profile at $T = 250$ K and $H = 0.3$ T. Sigmoid function fits the step-like part of the scattering. The cut-off angle is shown. Inset: SANS map above the critical field, $T = 250$ K and $H = 0.3$ T.

consists of the strong diffuse scattering in the vicinity of the former Bragg peak and a round spot limited by the critical angle θ_C. The diffuse scattering at $\boldsymbol{Q} = \pm\boldsymbol{k}_s$ is maximal at $H \approx H_{c2}$ and strongly suppressed by increase of the field. According to Eq. (2) the spin-wave part of the scattering becomes narrower with further increase of the field and has vanished at a certain H_{off} above H_{c2}. Using Eq.1, we define this value as

$$\theta_0^2 - \frac{\theta_0}{E_i}H_{off} = 0 \tag{4}$$

and obtain $H_{off} = \theta_0 E_i$. To define the cut-off angle θ_C, a measurement of the background intensity at $H > H_{off}$ was subtracted from the other scattering maps. To improve the statistics, the scattering intensity was azimuthally-averaged over the angular sector of 120 degrees with the center positioned at $\boldsymbol{Q} = \pm\boldsymbol{k}_s$, as shown in Fig.2. The resultant curve is shown in Fig.2 for $T = 250$ K and $H = 0.25$ T. From the analysis of the I versus $\theta - \theta_B$ plot the cut-off angle can be extracted.

Nevertheless, a sharp cut-off of the intensity was not observed due to the dumping of spin-waves. The expected step-like intensity profile is smeared into the smoothly decreasing curve. This smeared step-like edge of the measured intensity was fitted by the following sigmoid function, which captures the main features of the scattering:

$$I(\theta) = I_0\left\{\frac{1}{2} - \left(\frac{1}{\pi}\arctan\left[\frac{2\,(\theta-\theta_C)}{\delta}\right]\right)\right\} \tag{5}$$

The position of the cut-off angle was determined as the center of the arctan function θ_C. Its width δ is related to the spin-wave damping Γ.

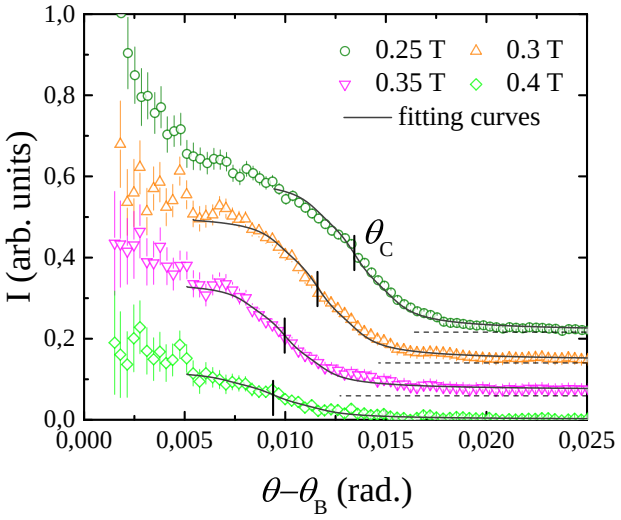

FIG. 3: (color online). The azimuthally averaged intensities at $T = 250$ K for different magnetic field between $H = 0.25$ T and $H = 0.4$ T. The fitting functions are chosen analogously to Fig.2. The curves are shifted by a constant with respect to each other for clarity.

Fig.3 shows the intensities as function of the angle $\theta - \theta_B$ at different values of the magnetic field for $T = 250$ K together with the corresponding fitting curves. The curves show a decrease of the value of the cut-off angle together with a strong suppression of the scattering $\theta \approx \theta_B$ with increase of the field. The latter is related to the gap in the spin-wave spectrum increasing with the field, when the quasi elastic scattering with relatively low ω is forbidden. Consequently, the intensity being proportional to $1/\omega$ decreases at low $(\theta - \theta_B)$.

The intensity for $H = 0.35$ T is plotted in Fig.4 (a) for different temperatures between 196 K and 270 K including fitting functions. Two parameters θ_c and δ have been extracted from the fitting procedure. Fig.4 (c) shows the field dependence of the dumping related parameter δ for different temperatures between 246 K and 277 K, which is nearly constant for each temperature. Fig.4 (b) shows the temperature dependence of δ, δ increases drastically close to T_C in accordance with theoretical expectations. The linear field dependence of the squared cut-off angle θ_C^2 against the magnetic field is shown in Fig.5 for $T =$ 246, 265 and 274 K. We were not able to determine the cut-off angle for the temperatures below 225 K because of the intensive quasi-elastic scattering arising in the position of the former Bragg peak position.

The square of the cut-off angle depends linearly on the field in accordance with Eq. (2). With the help of Eq. (2) one can determine the value of the parameter θ_0 and determine the spin-wave stiffness with high accuracy. The spin-wave stiffness, obtained from the cut-off angle for different temperatures is shown in Fig.6. The measured temperature dependence was fitted by the power law: $A(T) = a\,(1 - c\,(T/T_C)^z)$, parameters are found

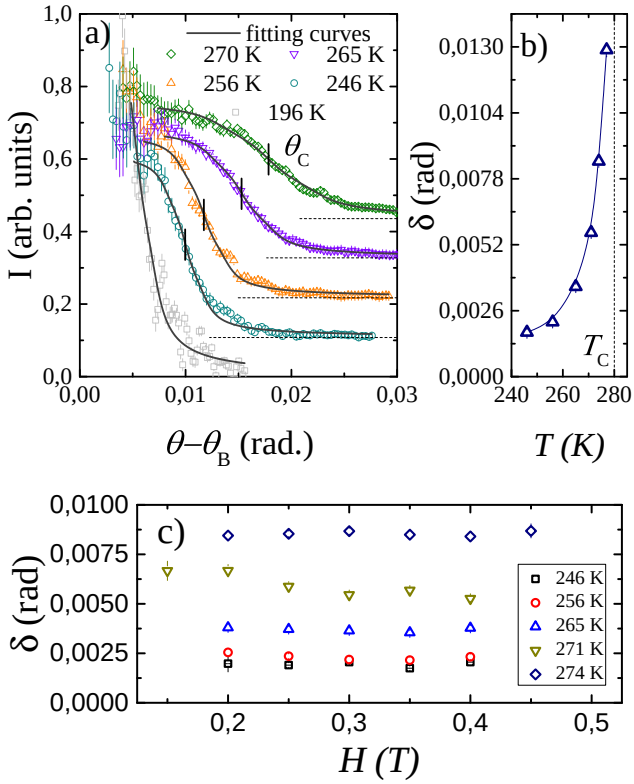

FIG. 4: (color online). (a) The temperature evolution of the intensity profiles from $T = 196$ K to $T = 270$ K at $H = 0.35$ T. The curves are shifted by a constant with respect to each other for clarity. (b) The relative change of width of the step-like part δ for $H = 0.35$. (c) The relative change of width of the step-like part δ for $T = 246K - 277K$ between $H = 0.15$ - 0.45 T.

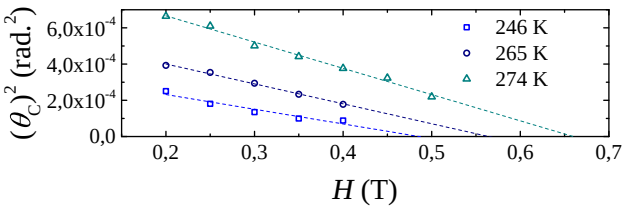

FIG. 5: (color online). The field dependence of the square of the cut-off angle θ_c^2 at $T = 246$ K, 265 K and 274 K. The intersections between the linear fits and the H axis determine H_{off}.

to be $a = (0.194 \pm 0.010)$ eVÅ^2, $c = 0.70 \pm 0.01$ and $z = 4.20 \pm 0.48$. The value of the stiffness A does not tend to 0 as one would expect at T_C, for the second order phase transitions, but is finite $A\,(T_C) = a \cdot 0.3 = 0.058$ eVÅ^2. This fact clearly classifies the magnetic phase transition in FeGe as being of the first order.

The spin-wave stiffness can also be estimated from the theory by Bak and Jensen[6] using the ratio relating the critical magnetic field H_{c2} and the difference in the energies between the FP and helical states $g\mu_B H_{c2} = Ak_s$. The relation has been experimentally confirmed to be

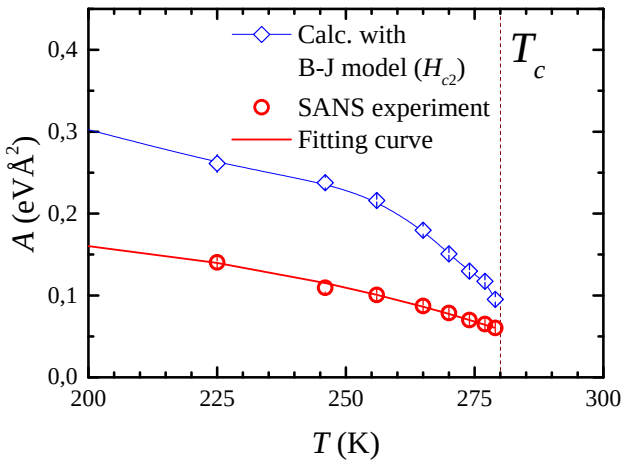

FIG. 6: (color online). Temperature dependence of the spin-wave stiffness: open red circles measured by the cut-off angle with the corresponding fit, blue diamonds values estimated by the Bak-Jensen model using critical field H_{c2}.

valid for MnSi in the whole temperature range below T_C[16]. The temperature dependence of the stiffness calculated in this model is also shown in Fig.6. The trend of the stiffness is the same including its decrease with temperature for the calculated and measured values. However, the magnitudes strongly deviate one from another. As the matter of fact, the probed excitations show two times lower value than it was predicted from the value of the H_{c2}. The discrepancy between the experimental and calculated value of A may be caused by the demagnetization effect within our polycrystalline samples, which has not been taken into account in determination of the critical field H_{c2}. Due to the higher magnetic moment and the polycrystalline nature of the used FeGe samples, this effect might play a bigger role for FeGe than for the previous investigated single crystalline MnSi[16].

IV. CONCLUSION

In conclusion, we have experimentally determined the spin-wave dynamic in the high temperature phase of the FeGe compound. We confirm the validity of the spin-wave dispersion relation for another helimagnet with DM interaction (Eq.(1)). Furthermore we demonstrated the ability of small-angle neutron scattering to measure the spin-wave dynamic in polycrystalline samples of DM helimagnets in the full-polarized state with acceptable statistics in reasonable time. The method allows the determination of the spin-wave dynamic in a broad temperature range and above all opens up complete new possibilities in the investigation of the parameter of the spin-wave dynamics in other representatives of DM helimagnets, which could be synthesized as powder only.

We thank Prof. S.V. Maleyev for valuable discussions and Prof. A. Schreyer for continuous interest and support. The work was supported by the Russian Foundation of Basic Research (Grant No 14-22-01073,14-02-00001) and the special program of the Department of Physical Science, Russian Academy of Sciences.

[1] I.E. Dzyaloshinskii, *Zh. Eksp. Teor. Fiz.* **46** 1420 (1964).
[2] T. Moriya, *Phys. Rev.* **120**, 91 (1960).
[3] P. Bak, M.H. Jensen, *J.Phys.* **C13** L881 (1980).
[4] O. Nakanishia, A. Yanasa, A. Hasegawa, M. Kataoka *Solid State Commun* **35** 995-998 (1980).
[5] S. V. Grigoriev, A. S. Sukhanov and S. V. Maleyev *Phys. Rev. B* **91** 224429 (2015).
[6] S. V. Maleyev, *Phys. Rev. B* **73** 174402 (2006).
[7] B. Lebecht, J. Bernhard and T. Freltloft *J.Phys.: Condens. Matter* **1** 6105-6122 (1989).
[8] Y. Ishikawa, K. Tajima, D. Bloch and M. Roth *Solid State Commun.* **19** 525 (1979).
[9] L. Lundgren, O. Beckman, V. Attia, S. P. Bhattacherjee and M. Richardson. *Physica Scripta* **1** 69-72 (1970).
[10] Y. Ishikawa, G. Shirane, J. A. Tarvin, and M. Kohgi *Phys. Rev. B* **16**, 4956 (1977).
[11] J. A. Tarvin, G. Shirane, Y. Endoh, and Y. Ishikawa *Phys. Rev. B* **18** 4815 (1978).
[12] F. Semadeni, P. Boni, Y. Endoh, B. Roessli, and G. Shirane *Physica B* **248** 267-268 (1999).
[13] M. Janoschek, F. Bernlochner, S. Dunsiger, C. Pfleiderer, P. Boni, B. Roessli, P. Link, and A. Rosch *Phys. Rev. B***81** 214436 (2010).
[14] M. Kugler, G. Brandl, J. Waizner, M. Janoschek, R. Georgii, A. Bauer, K. Seemann, A. Rosch, C. Pfleiderer, P. Boni, and M. Garst, *Phys. Rev. Lett.* **115** 097203 (2015).
[15] T. Schwarze, J. Waizner, M. Garst, A. Bauer, I. Stasinopoulos, H. Berger, C. Pfleiderer and D. Grundler *Nature Materials* **14** 478483 (2015).
[16] S. V. Grigoriev, A. S. Sukhanov, E. V. Altynbaev, S.-A. Siegfried, A. Heinemann, P. Kizhe, and S. V. Maleyev *Phys. Rev. B* **92** 220415(R) (2015).
[17] A. I. Okorokov, V. V. Runov, B. P. Toperverg, A. D. Tretyakov, E. I. Maltsev, I. M. Puzeii, and V. E. Mikhailova, Pis'ma v ZhETF 43, 390 (1986) [JETP Lett. 43, 503 (1986)].
[18] V. Deriglazov, A. Okorokov, V. Runov, B. Toperverg, R. Kampmann, H. Eckerlebe, W. Schmidt, and W. Lobner *Physica B* **262** 180-181 (1992).
[19] B. P. Toperverg, V. V. Deriglazov, and V. E. Mikhailova *Physica B* **183** 326 (1993).
[20] S. V. Grigoriev, S. V. Maleyev, V. V. Deriglazov, A. I. Okorokov, N. H. van Dijk, E. Bruck, J. C. P. Klaasse, H. Eckerlebe, and G. Kozik *Appl. Phys. A* **74** s719 (2002).
[21] S. V. Grigoriev, E. V. Altynbayev, H. Eckerlebe, and A. I. Okorokov *J. Surf. Invest.: X-Ray, Synchrotron Neutron Tech.* **8** 1027 (2014).
[22] M. Kataoka, Jour. Phys. Soc. Jap., **56**, No 10 3635-3647

(1987).
[23] S. V. Grigoriev, S.-A. Siegfried, E. V. Altynbayev, N. M. Potapova, V. Dyadkin, E. V. Moskvin, D. Menzel, A. Heinemann, S. N. Axenov, L. N. Fomicheva, and A. V. Tsvyashchenko *Phys. Rev. B* **90** 174414 (2014).
[24] A. Tsvyashchenko, *J. Less Common Metals* **99** L9 (1984).